Physics of the Earth and Planetary Interiors 232 (2014) 51–56

Contents lists available at ScienceDirect

Physics of the Earth and Planetary Interiors

journal homepage: www.elsevier.com/locate/pepi

# The effect of pressure on the electrical conductivity of olivine under the hydrogen-rich conditions

Lidong Dai [a,b], Shun-ichiro Karato [b,*]

[a] Laboratory for High Temperature and High Pressure Study of the Earth's Interior, Institute of Geochemistry, Chinese Academy of Sciences, Guiyang, Guizhou 550002, China
[b] Department of Geology and Geophysics, Yale University, New Haven, CT 06511, USA

ARTICLE INFO

*Article history:*
Received 5 November 2013
Received in revised form 7 March 2014
Accepted 24 March 2014
Available online 2 April 2014

*Keywords:*
Electrical conductivity
Polycrystalline olivine
Pressure
Water

ABSTRACT

The influence of pressure on the hydrogen-assisted electrical conductivity in olivine has been studied under conditions of 4–10 GPa and 873–1273 K. Synthetic polycrystalline olivine samples with the water content of 160 ppm wt (Paterson calibration) were used and the electrical conductivity was determined from the results of the impedance spectroscopy. We found that the pressure reduces the hydrogen-assisted electrical conductivity, but its magnitude is small: between 4 and 10 GPa, the difference is a factor of ~2.5 for the same water content and temperature. The pressure dependence is characterized by a negative activation volume and the negative dependence of the pre-exponential factor on pressure. Such anomalous behavior is explained by a model where hydrogen-related defect is considered as a weak inclusion in a strong matrix.

We use these new data to calculate the electrical conductivity contrast at the 410-km discontinuity. We found that if the water content of the mantle does not change with depth, there should be a large (a factor of ~10) drop in conductivity from above to below the 410-km discontinuity. In contrast, geophysically inferred electrical conductivity increases at 410-km suggesting the increase in water content from above to below the 410-km discontinuity.

The present results are used to compare several previous results obtained at different pressures. It was shown that our results agree well with most of previous studies but not with (Yoshino et al., 2009). Possible causes for this discrepancy are discussed.



## 1. Introduction

Although the role of hydrogen in electrical conductivity in olivine has been extensively studied (e.g., (Poe et al., 2010; Wang et al., 2006; Yang, 2012; Yoshino et al., 2009; Yoshino et al., 2006)), the influence of pressure on hydrogen-assisted electrical conductivity has not been investigated. Consequently, it was difficult to compare experimental results on olivine obtained at different pressures. For example, (Karato, 2011) noted that the results by Yoshino et al. (2009) are systematically different from those by Wang et al. (2006) and discussed that the difference between the results by Wang et al. (2006) and Yoshino et al. (2009) might be caused by the pressure effect (the former study was at 4 GPa shows higher conductivity than the latter measured was at 10 GPa). Similarly, in order to compare previous studies on olivine conductivity (Poe et al., 2010; Wang et al., 2006; Yang, 2012; Yoshino et al., 2009), one needs to know the pressure effects, because these studies were performed at a broad range of pressure (1–10 GPa).

In addition, the estimation of the conductivity-depth profile has been hampered by the lack of the data on the pressure effect on hydrogen-assisted electrical conductivity in olivine. For example, (Karato, 2011) used two different models to estimate the electrical conductivity profiles for the whole upper mantle, one with no pressure effect, and another with a large pressure effect assuming that the difference between Wang et al. (2006) and Yoshino et al. (2009) was due to the pressure effect. The difference between these two models is large making it difficult to estimate the water distribution across the 410-km discontinuity.

The aims of the present study are to address these two issues, i.e., (1) to evaluate the expected conductivity jump at the "410-km" discontinuity for a constant water content model, and (2) to compare various studies normalized to the same pressure (of 8.0 GPa) to identify the source of discrepancy noted in the previous studies.

* Corresponding author. Tel.: +1 203 432 3147; fax: +1 203 432 3134.
*E-mail address:* shun-ichiro.karato@yale.edu (S.-i. Karato).

http://dx.doi.org/10.1016/j.pepi.2014.03.010
0031-9201/

## 2. Experimental procedure

### 2.1. Sample preparation

The hydrous polycrystalline olivine samples were synthesized from San Carlos olivine powders with the grain size less than 5 micron by hydrothermal annealing experiments at $P = 4$ GPa and $T = 1473$ K for 3 hrs. About 1.85 wt% of San Carlos orthopyroxene was added to buffer the oxide activity. Powder samples of olivine and orthopyroxene mixture were sealed into a nickel capsule. Both synthesis and conductivity measurements were performed using the same Ni-NiO solid oxygen buffer. Our previous experiences indicated that under these environments, the oxidation conditions of samples are well buffered by the metal and its corresponding metal oxide reactions (e.g., Nishihara et al., 2006, 2008; Dai and Karato, 2009b). We obtained dense polycrystalline olivine with ~160 ppm wt water content. The details of hydrothermal experiments are described by Wang et al. (2006). The FT-IR spectroscopy of hydrothermally treated samples shows homogeneously distributed hydrogen.

### 2.2. Sample characterization

In order to determine the water content of the samples, the infrared spectra of samples were obtained at wavenumbers from 1000 to 4000 $cm^{-1}$ both before and after each experiment. The measurements were made using a Fourier transform infrared spectroscopy (FT-IR) spectrometer (BIORAD, Varian 600 UMA). Doubly polished samples with a thickness of less than 120 μm were prepared for the IR analysis. The IR absorption of samples was measured by unpolarized radiation with a mid-IR light source, a KBr beam splitter and an MCT detector with a 120 × 120 $\mu m^2$ aperture, so a volume sampled by an IR beam contains a few thousand of grains. 512 scans were accumulated for each sample. The infrared spectra of the acquired samples are shown in Fig. 1. We used the Paterson (1982) calibration to determine the water content from FT-IR absorption using,

$$C_{OH} = \frac{B_i}{150\xi}\int \frac{K(\nu)}{(3780-\nu)}d\nu \quad (1)$$

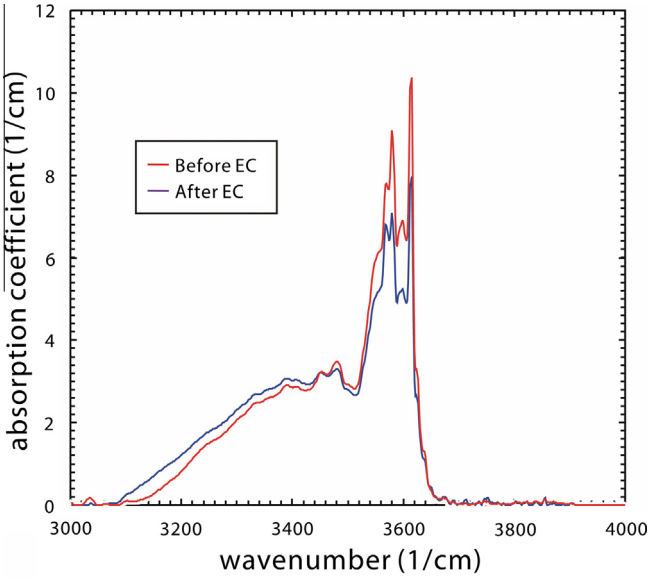


**Fig. 1.** The representative FT-IR spectra of olivine aggregate before and after electrical conductivity measurement (at 7 GPa) for the wavenumber range of 3000–4000 $cm^{-1}$.

where $C_{OH}$ is the molar concentration of hydroxyl (ppm wt $H_2O$ or H/$10^6$ Si), $B_i$ is the density factor ($4.39 \times 10^4$ cm H/$10^6$ Si), $\xi$ is the orientation factor (1/2), and $K(\nu)$ is the absorption coefficient in $cm^{-1}$ at wavenumber $\nu$ in $cm^{-1}$. The integration was made from 3000 to 3750 $cm^{-1}$ to avoid the influence of a singularity that occurs at 3780 $cm^{-1}$. If another calibration such as (Bell et al., 2003) is used, the water content will be larger by a factor of ~3. Although there are some issues with using unpolarized FTIR spectroscopy (e.g., Withers, 2013), this issue is not serious in our case because a large number of nearly randomly oriented grains are sampled.

The water content of the original sample is less than 8 H/$10^6$ Si (0.0001 wt% $H_2O$). After the olivine was annealed under the hydrous environment, one sample containing different water contents of ~160 ppm wt was obtained. The water loss during the electrical conductivity measurements of hydrous sample was less than 8%.

### 2.3. Impedance spectroscopy measurements

The experimental sample assembly is shown in Fig. 2. Pressure was generated by eight cubic tungsten carbide anvils ($26 \times 26 \times 26$ $mm^3$) with a 14–18 mm truncated edge length depending on the pressure. Pressure calibrations were conducted using the phase transitions of coesite to stishovite (Zhang et al., 1996, 9.5 GPa and 1573 K), as well as forsterite to wadsleyite (Morishima et al., 1994, 14 GPa and 1573 K). In order to avoid the influence of adsorbed water on the measurement of electrical conductivity, all sample assembly parts were heated to 1223 K for 12 hrs prior to each experiment. In order to control the oxygen fugacity of the sample chamber and reduce the leakage currents, a Ni foil shield was placed between a sample and an MgO insulation tube. A disk-shaped sample (Φ1.6 × 0.4 mm) was placed between two parallel Ni electrodes that were surrounded by alumina rings. The temperature was measured by a $W_{5\%}Re$–$W_{26\%}Re$ thermocouple that is attached to another side of Ni electrode (Ni is in direct contact with a sample). The experimental errors of the pressure and temperature gradient were estimated to be at no more than 0.5 GPa and 10 K, respectively (absolute error in pressure estimate can be larger but the relative error is ~0.5 GPa or less). The errors in electrical conductivity measurement through the impedance fitting were estimated to be less than 3%.

The pressure was first raised at the rate of ~0.9 GPa/h to a designated pressure. Under a constant pressure condition, temperature was raised at the rate of ~50 K/min to the preset value and

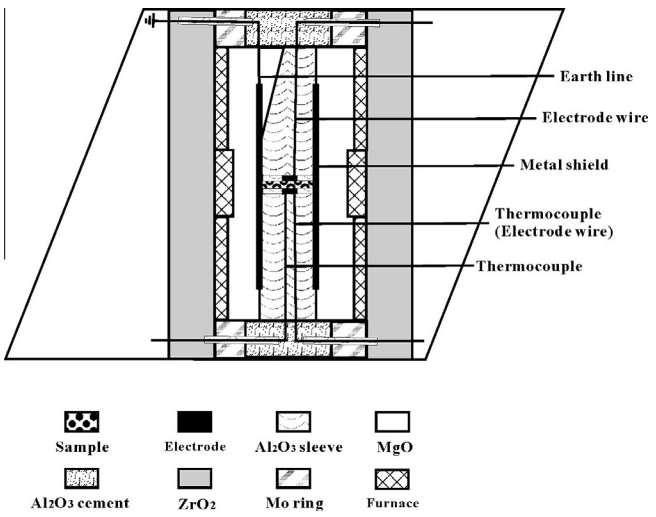


**Fig. 2.** The experimental setup for electrical conductivity measurements at high pressure and temperature.

the impedance spectroscopy measurements were performed at various temperatures. After the temperature reached to an each value for a constant pressure condition, the ZPlot program of a Solartron-1260 Impedance/Gain-Phase analyzer was run to determine the complex impedance for the frequency range of $f = 10^{-2}$–$10^{6}$ Hz for a sinusoidal alternating current of signal voltage of 1.0 V. The impedance semi-circle arc of high frequency branch ($10^{6}$–$10^{3}$ Hz) was fitted by virtue of an equivalent circuit of the ZView program that was made up of a resistor connected in parallel with a capacitor. From the fitting of the semi-circle to this model, we determined the conductivity of a sample. In most of the runs, the conductivity was determined with decreasing temperature after the peak temperature was reached. All experimental conditions including water content before and after each experiment, pressure and temperature are summarized in Table 1.

## 3. Results

The representative impedance spectroscopy results at conditions of 7 GPa, 873–1273 K and the water content of ~160 ppm wt is shown in Fig. 3. Results obtained under other conditions are qualitatively similar to those illustrated here. We observed two circles at high temperatures, whereas only one circle was observed at low temperatures. The presence of two circles in the impedance spectroscopy implies two processes of charge transfer and blocking. The first circle originated at the origin ($Z' = Z'' = 0$) likely corresponds to a parallel combination of resistor and capacitor, and the second circle likely represents the conduction process between sample and electrode (Bagdassarov et al., 2011; Barkmann and Cemič, 1996). The presence of a capacitor in the impedance response implies that there are mechanisms to accumulate electric charge in the sample. They include the charge transfer at the sample-electrode interface and the blocking of charge transfer at grain-boundaries.

The electrical conductivities of the samples were calculated using the following equation,

$$\sigma = \frac{L/S}{R} = \frac{L}{SR} \tag{2}$$

where $L$ is the sample length and $S$ is the cross section area of the electrode. Both $L$ and $S$ are determined before and after each experiment and only small changes in $L$ and $S$ are observed (less than ~5% including the influence of pressure). The relationship between the electrical conductivity and temperature were found to satisfy the Arrhenius relation,

$$\sigma = A(P) \cdot \left(\frac{C_w}{C_{wo}}\right)^{r} \cdot \exp\left(-\frac{E^* + PV^*}{RT}\right) \tag{3}$$

where $A$ is the pre-exponential factor that is approximately independent of temperature (S/m), $C_w$ is water content, $C_{wo}$ is the reference water content (160 ppm wt, Paterson calibration), $E^*$ is activation energy and $V^*$ is activation volume, $P$ is pressure, $T$ is temperature and $R$ is the gas constant. As can be seen in Fig. 4, there is a marked pressure dependence of the pre-exponential factor ($A$), so $A$ is assumed to depend on pressure as $A = A_0(1\text{-}BP)$ where $B$ is a constant with a dimension of 1/GPa.

**Table 1**
Summary of runs.

| Run # | P (GPa) | T (K) | Water content (ppm H/Si)[a] | |
|---|---|---|---|---|
| | | | Before experiment | After experiment |
| K1318 | 4 | 873–1273 | 2335 | 2317 |
| K1321 | 7 | 873–1273 | 2326 | 2296 |
| K1323 | 10 | 873–1273 | 2329 | 2434 |

[a] Paterson (1982) calibration.

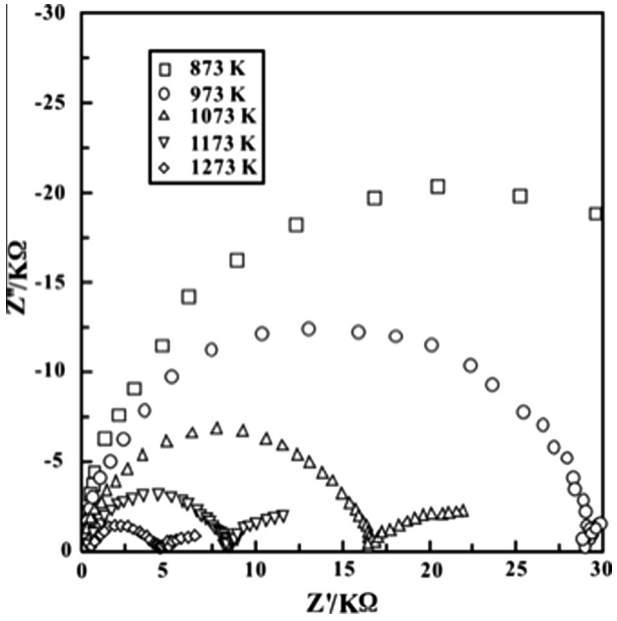


**Fig. 3.** A $Z'$ vs. $Z''$ plot of complex impedance of hydrous olivine aggregates from $10^{-2}$ to $10^{6}$ Hz (right to left), obtained under conditions of 7.0 GPa, 873–1273 K and 160 ppm wt water content (Paterson calibration). $Z'$ and $Z''$ are the real and imaginary part of complex impedance respectively.

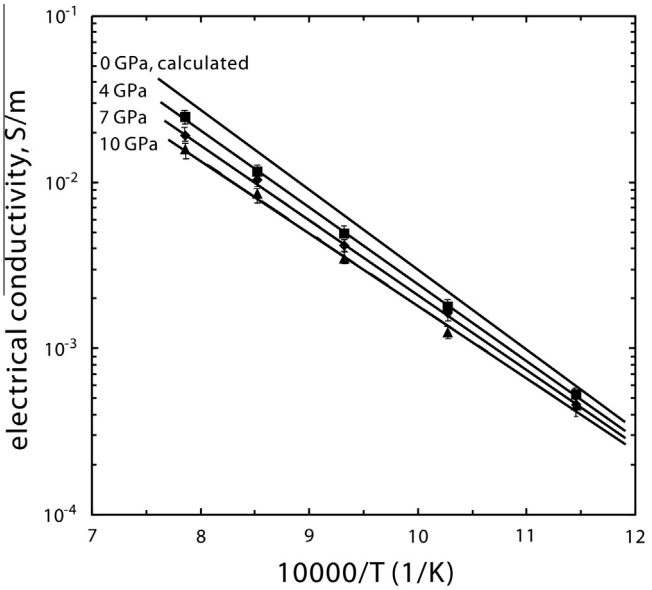


**Fig. 4.** Influence of pressure on the electrical conductivity of hydrous olivine aggregates at the temperature of 873–1273 K. Fitting data at 4, 7 and 10 GPa yields the parameters in Table 2. The bars indicate errors.

The obtained fitted results for electrical conductivity are listed in Fig. 4 and Table 2. With increasing pressure, the electrical conductivity of hydrous olivine decreases, the pre-exponential factor slightly decreases, and the activation enthalpy also decreases.

## 4. Discussion

### 4.1. Comparison with previous studies

There are some studies on the influence of pressure on electrical conductivity. The influence of pressure on the polaron conduction in San Carlos olivine single crystal was studied by Xu et al. (2000)

**Table 2**
Parameter values for the electrical conductivity of hydrous polycrystalline olivine (units: $A$: S/m, $E^*$: kJ/mol, $V^*$: cm$^3$/mol, $P$: GPa). The relation $\sigma = A \cdot \left(\frac{C_w}{C_{wo}}\right)^r \cdot \exp\left(-\frac{E^*+PV^*}{RT}\right)$ is employed to globally fit the data (the non-linear fitting program of Origin™ was used). In view of the strong dependence of experimental data of $A$ value on pressure, we used a relation $A = A_0(1\text{-}BP)$ (where the unit for B is 1/GPa). Errors are one standard deviation, and include the contribution of errors in individual measurements (errors in water content, temperature and electrical conductivity).

| | A | $E^*$ (kJ/mol) | $V^*$ (cm$^3$/mol) |
|---|---|---|---|
| Paterson calibration | $A_0$ = 189 ± 12 (S/m)<br>$B$ = 0.028 ± 0.003 (1/GPa) | 92 ± 4 | −0.86 ± 0.05 |
| Bell calibration | $A_0$ = 96 ± 8 (S/m)<br>$B$ = 0.028 ± 0.003 (1/GPa) | | |

under conditions of 4–10 GPa, 1273–1673 K and a Mo-$MoO_2$ oxygen fugacity buffer. In addition, the influence of pressure on both proton and hopping conduction was studied for pyrope garnet by Dai and Karato (2009a). In all cases, the influence of pressure is relatively small: a change in pressure by $\Delta P$ = 5 GPa results in the change in conductivity by less than a factor of ~2.5.

Given this new result on the pressure effects on electrical conductivity in hydrous olivine, we can now compare results obtained at different pressures. We compare five studies where electrical conductivity of hydrous olivine was studied. The pressure at which these studied was made ranges from 1 GPa to 10 GPa (see Table 3), and hence the correction for the pressure effect is potentially important. In order to minimize the extrapolation, we chose the water content of 160 ppm wt (480 ppm wt if the Bell calibration is used) olivine aggregates in the present studies. When we compare results from different water content, the influence of water content is corrected assuming $\sigma \propto C_w^r$ with $r$ = 0.62 (Wang et al., 2006). Somewhat different values of $r$ were reported, but because this reference water content is close to the water content where most of the previous measurements were made, the influence of this correction is not large. Also when different water content calibrations were used, we made a correction for the different conversion factors. The results are shown in Fig. 5.

Fig. 5 show that the results by Poe et al. (2010), Wang et al. (2006), Yang (2012) agree well (with a factor of 2–3) whereas the results by Yoshino et al. (2009) are much lower than these results (we did not compare with the results by (Yoshino et al., 2006) where conductivity was estimated only by one low frequency measurement and hence the results have systematic bias caused by the influence of polarization effect; see (Karato and Dai, 2009)). Yoshino et al. (2009)'s results show the electrical conductivity that is lower than those calculated from H-D isotope diffusion (at temperatures higher than ~1300 K) (Karato, 2013). This is theoretically not plausible, because the electrical conductivity calculated from the isotope diffusion coefficients provides the lower limit (Karato, 2013). Karato (2011) discussed the influence of pressure might be a cause of this large discrepancy. However, the possibility of pressure effect can be ruled out from our new results reported here.

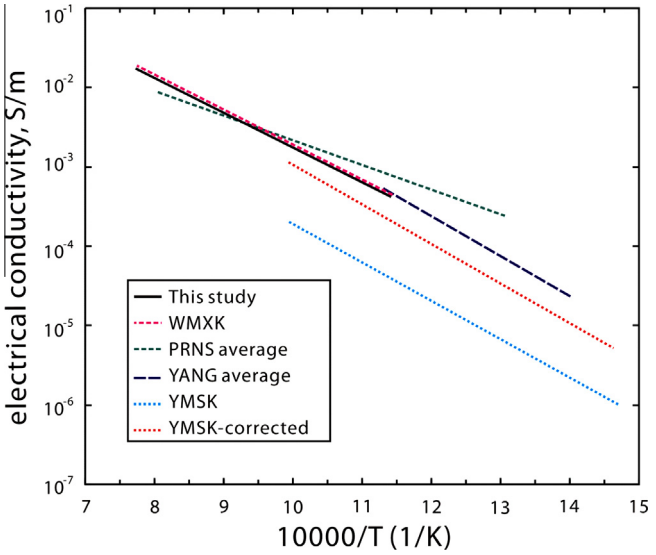


**Fig. 5.** A comparison of several previous experimental results on hydrogen-assisted electrical conductivity of olivine. A comparison is made at a common water content of 160 ppm wt (for the Paterson calibration; some studies used the Bell calibration. In these cases, a comparison is made at the same water content after a correction for the calibration). The data from different water content is normalized using the relation, $\sigma \propto C_w^r$ with $r$ = 0.62. Data sources: Solid lines = the present study, the pink dashed line (WMXK): for polycrystalline aggregates from Wang et al. (2006), the green dashed line (PRNS): averaged along ||a, ||b and ||c single crystals from Poe et al. (2010), the purple dashed line (YANG): averaged along ||a, ||b and ||c single crystals from Yang (2012), the blue dashed line (YMSK): for polycrystalline sample by Yoshino et al. (2009), and red dashed line (YMSK-corrected): for polycrystalline aggregates from Yoshino et al. (2009) corrected for the water content (see text). (For interpretation of the references to color in this figure legend, the reader is referred to the web version of this article.)

We note that in Table 1 of Yoshino et al. (2009), the water contents of all the samples are shown both for wt% and ppm H/Si units. However, these values do not match each other. The values in wt% are 10 times larger than they should be if these values were converted from ppm H/Si. Consequently, we show a comparison for both the raw data from Yoshino et al. (2009) and corrected values (by a factor of 10). The results for corrected water content agree reasonably well with other data, but uncorrected values do not.

Another possibility is the difference in the water content calculation between our lab and Yoshino's lab. In our lab, we apply the base-line correction and integrate absorbance from 3000 to 3750 cm$^{-1}$ to avoid a singularity at 3780 cm$^{-1}$. This singularity is unphysical and for a practical purpose, one should avoid integrating beyond this wave number. It is unclear how Yoshino's group calculates the water content from FTIR absorption spectra.

### 4.2. Implications for conductivity mechanisms

The observed small effects of pressure (at the same hydrogen content) are similar to that found for hydrogen-assisted electrical

**Table 3**
Comparisons with previous results on the electrical conductivity of hydrous olivine.

| Source | Sample | $P$ (GPa) | $T$ (K) | Frequency (Hz) | Shield | Water content (ppm wt%) |
|---|---|---|---|---|---|---|
| This study | Polycrystalline aggregate | 4–10 | 873–1273 | $10^{-2}$–$10^{6}$ | Y | 160[a] |
| Wang et al. (2006) | Polycrystalline aggregate | 4 | 873–1273 | $10^{3}$–$10^{6}$ | Y | 100–800[a] |
| Poe et al. (2010) | ||a, ||b and ||c single crystal | 8 | 773–973 | $10^{-1}$–$10^{5}$ | Y | 363–2215[b] |
| Yang et al. (2012) | ||a, ||b and ||c single crystal | 1 | 623–973 | $10^{-1}$–$10^{6}$ | Y | 40[b] |
| Yoshino et al. (2009) | Polycrystalline aggregate | 10 | 500–1000 | $10^{-1}$–$10^{6}$ | N | 50–1700[a] |

[a] Paterson (1982) calibration.
[b] Bell et al. (2003) calibration.

conductivity in other minerals such as pyrope garnet. Although a negative activation energy may be expected for electronic conduction (because of the enhanced overlap of electron orbits by compression), the negative activation volume (and the reduction of the pre-exponential factor $A_o$ with pressure) is anomalous in comparison to what are observed normally in diffusion of atoms in solids (e.g., Karato, 1981; Sammis et al., 1981). A possible explanation is to consider a hydrogen-related defect as a soft region in a (hard) matrix (such a model is supported by the observations on the elastic constants (e.g., Jacobsen et al., 2008; Karato, 1995)).

If one uses a strain energy model of defect energy ($G^* \propto C\Omega$; (Keyes, 1963); $C$: elastic constant of a defect region, $\Omega$: volume of a defect), the Nernst–Einstein relation, $\sigma = \frac{Dcq^2}{RT}$ ($D$: diffusion coefficient, $c$: number density of the charged particle, $q$: the electric charge of the particle), and a model of diffusion where the pre-exponential factor is proportional to $a^2\nu$ ($a$: lattice constant, $\nu$: vibrational frequency), then one obtains,

$$\frac{\partial \log A}{\partial P} = \frac{1}{2K}\left(\frac{\partial \log C}{\partial \log \rho} - \frac{1}{3}\right) \quad (4)$$

and

$$\frac{\partial \log G^*}{\partial P} = \frac{V^*}{G^*} = \frac{1}{K}\left(\frac{\partial \log C}{\partial \log \rho} - 1\right) \quad (5)$$

where $\rho$ is density. It is seen that if $\frac{\partial \log C}{\partial \log \rho} < 1$, then $V^*<0$ and $\frac{\partial A}{\partial P} < 0$. In a normal material, $\frac{\partial \log C}{\partial \log \rho} = 2\gamma + \frac{1}{3} = 2.5 - 3.5$ (e.g., Karato, 2008) and $V^*>0$ for ionic conductivity. However, for a weak defect embedded in a hard matrix, the elastic constant of defect does not change upon compression as much as it would be if the defect existed in isolation because the volume change of a weak defect region surrounded by a strong matrix is smaller than it would be without the matrix. In such a case, one can write $\frac{\partial \log C}{\partial \log \rho} = \left(\frac{\partial \log C}{\partial \log \rho}\right)_o \xi$ where $\left(\frac{\partial \log C}{\partial \log \rho}\right)_o$ is $\frac{\partial \log C}{\partial \log \rho}$ for a normal (homogeneous) material and $\xi$ is a non-dimensional parameter that represents the influence of a strong matrix to reduce the volume change of a weak defect region. This parameter depends on the elastic constant ratio between the inclusion (defect region) and the matrix (Eshelby, 1957). If the bulk modulus of a defect (hydrogen-oxygen complex) is much weaker than that of the matrix, $\xi \ll 1$ leading to a negative activation volume and $\frac{\partial A}{\partial P} < 0$ .

### 4.3. Estimation of the electrical conductivity jump at the "410-km" discontinuity

Given the new results on the pressure dependence of hydrogen-assisted conductivity, we can calculate the conductivity-depth profile for the whole upper mantle using plausible geotherm, for a range of assumed water content. We used the geotherm model by Katsura et al. (2010). The method of calculation is the same as the one used by Karato (2011) where the influence of depth variation of oxygen fugacity, and the influence of hydrogen partitioning among co-existing phases are included. Because the electrical conductivity assisted by hydrogen is similar among these three minerals at the same temperature, pressure and water content (Karato and Wang, 2013), the influence of hydrogen partitioning is small. For the transition zone, we used the results by Dai and Karato (2009a).

The main difference between Karato (2011) and the present study is that we now use the experimental data on the influence of pressure on hydrogen-assisted conductivity. Our new results show only small pressure effects and consequently the results are similar to Karato (2011) with no pressure effect: there is a substantial drop in electrical conductivity at 410 km from the upper mantle and the transition zone if the water content in these regions are the same (Fig. 6). In contrast, the actually inferred

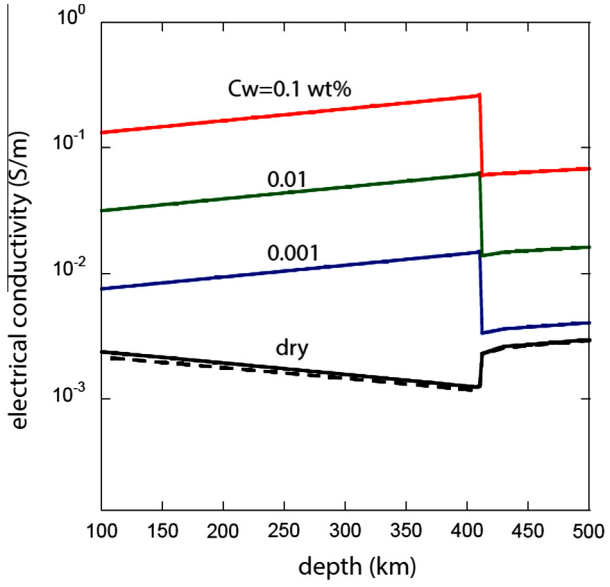


**Fig. 6.** Electrical conductivity ($\sigma$) versus depth relationships for the upper mantle and mantle transition zone calculated from the geotherm of Katsura et al. (2010) for the pyrolite mantle model with various water contents. Solid (broken) lines correspond to the Hashin–Shtrikman upper (lower) bounds. For hydrogen conduction, the upper and the lower bounds are indistinguishable. Data source: conductivity data at a depth from 100 km to 410 km is obtained from our current hydrous polycrystalline aggregates, and conductivity data at a depth from 410 km to 500 km are obtained from Dai and Karato (2009a). The water content is based on the Bell calibration. The conductivity in the shallow asthenosphere ($10^{-2}$–$10^{-1}$ S/m) can be attributed to ~0.01 wt% of water, whereas if the water content of the upper mantle were the same as that of the transition zone (below 410-km), then a conductivity drop would be observed.

electrical conductivity of the mantle transition zone is higher than the electrical conductivity of the upper mantle although large regional variations are present (e.g., Baba et al., 2010; Kelbert et al., 2009; Utada et al., 2003). We confirm the earlier notion that there is a substantial jump in the water content across the 410-km discontinuity (Karato, 2011).

## Acknowledgements

Robert Farla, George Amulele and Zhenting Jiang kindly provided technical guidance and assistance in the FT-IR measurement. This research was financially supported by the "135" Program of Institute of Geochemistry, CAS and NSF of China (41174079) and partly by NSF of United States.

## References

Baba, K., Utada, H., Goto, T., Kasaya, T., Shimizu, H., Tada, N., 2010. Electrical conductivity imaging of the Philippine Sea upper mantle using seafloor magnetotelluric data. Phys. Earth Planet. Inter. 183, 44–62.

Bagdassarov, N., Batalev, V., Egorova, V., 2011. State of lithosphere beneath Tien Shan from petrology and electrical conductivity of xenoliths. J. Geophys. Res. 116. http://dx.doi.org/10.1029/2009JB007125.

Barkmann, T., Cemič, L., 1996. Impedance spectroscopy and defect chemistry of fayalite. Phys. Chem. Miner. 23, 186–192.

Bell, D.R., Rossman, G.R., Maldener, J., Endisch, D., Rauch, F., 2003. Hydroxide in olivine: a quantitative determination of the absolute amount and calibration of the IR spectrum. J. Geophys. Res. 108. http://dx.doi.org/10.1029/2001JB000679.

Dai, L., Karato, S., 2009a. Electrical conductivity of pyrope-rich garnet at high temperature and pressure. Phys. Earth Planet. Inter. 176, 83–88.

Dai, L., Karato, S., 2009b. Electrical conductivity of wadsleyite under high pressures and temperatures. Earth Planet. Sci. Lett. 287, 277–283.

Eshelby, J.D., 1957. The determination of the elastic strain field of an ellipsoidal inclusion and related problems. Proc. R. Soc. London Ser. A 241, 376–396.

Jacobsen, S.D., Jiang, F., Mao, Z., Duffy, T.S., Smyth, J.R., Holl, C.M., Frost, D.J., 2008. Effects of hydration on the elastic properties of olivine. Geophys. Res. Lett. 35. http://dx.doi.org/10.1029/2008GL034398.

Karato, S., 1981. Pressure dependence of diffusion in ionic solids. Phys. Earth Planet. Inter. 25, 38–51.
Karato, S., 1995. Effects of water on seismic wave velocities in the upper mantle. Proc. Jpn. Acad. 71, 61–66.
Karato, S., 2008. Deformation of Earth Materials: Introduction to the Rheology of the Solid Earth. Cambridge University Press, Cambridge.
Karato, S., 2011. Water distribution across the mantle transition zone and its implications for global material circulation. Earth Planet. Sci. Lett. 301, 413–423.
Karato, S., 2013. Theory of isotope diffusion in a material with multiple-species and its implications for hydrogen-enhanced electrical conductivity in olivine. Phys. Earth Planet. Inter. 219, 49–54.
Karato, S., Dai, L., 2009. Comments on "Electrical conductivity of wadsleyite as a function of temperature and water content" by Manthilake et al.. Phys. Earth Planet. Inter. 174, 19–21.
Karato, S., Wang, D., 2013. Electrical conductivity of minerals and rocks. In: Karato, S. (Ed.), Physics and Chemistry of the Deep Earth. Wiley-Blackwell, New York, pp. 145–182.
Katsura, T., Yoneda, A., Yamazaki, D., Yoshino, T., Ito, E., 2010. Adiabatic temperature profile in the mantle. Phys. Earth Planet. Inter. 183, 212–218.
Kelbert, A., Schultz, A., Egbert, G., 2009. Global electromagnetic induction constraints on transition-zone water content variations. Nature 460, 1003–1006.
Keyes, R.W., 1963. Continuum models of the effect of pressure on activated processes. In: Paul, W., Warschauer, D.M. (Eds.), Solids Under Pressure. McGraw-Hills, New York, pp. 71–91.
Morishima, H., Kato, T., Suto, M., Ohtani, E., Urakawa, S., Utsumi, W., Shimomura, O., Kikegawa, T., 1994. The phase-boundary between $\alpha$-$Mg_2SiO_4$ and $\beta$-$Mg_2SiO_4$ determined by in-situ X-ray observation. Science 265, 1202–1203.
Nishihara, Y., Shinmei, T., Karato, S., 2006. Grain-growth kinetics in wadsleyite: effects of chemical environment. Phys. Earth Planet. Inter. 154, 30–43.
Nishihara, Y., Shinmei, T., Karato, S., 2008. Effects of chemical environments on the hydrogen-defects in wadsleyite. Am. Mineral. 93, 831–843.
Poe, B., Romano, C., Nestola, F., Smyth, J.R., 2010. Electrical conductivity anisotropy of dry and hydrous olivine at 8 GPa. Phys. Earth Planet. Inter. 181, 103–111.
Sammis, C.G., Smith, J.C., Schubert, G., 1981. A critical assessment of estimation methods for activation volume. J. Geophys. Res. 86, 10707–10718.
Utada, H., Koyama, T., Shimizu, H., Chave, A.D., 2003. A semi-global reference model for electrical conductivity in the mid-mantle beneath the north Pacific region. Geophys. Res. Lett. 30. http://dx.doi.org/10.1029/2002GL016092.
Wang, D., Mookherjee, M., Xu, Y., Karato, S., 2006. The effect of water on the electrical conductivity in olivine. Nature 443, 977–980.
Withers, A.C., 2013. On the use of unpolarized infrared spectroscopy for quantitative analysis of absorbing species in birefringent crystals. Am. Mineral. 98, 689–697.
Xu, Y., Shankland, T.J., Duba, A.G., 2000. Pressure effect on electrical conductivity of mantle olivine. Phys. Earth Planet. Inter. 118, 149–161.
Yang, X., 2012. Orientation-related electrical conductivity of hydrous olivine, clinopyroxene and plagioclase and implications for the structure of the lower continental crust and uppermost mantle. Earth Planet. Sci. Lett. 317 (318), 241–250.
Yoshino, T., Matsuzaki, T., Shatskiy, A., Katsura, T., 2009. The effect of water on the electrical conductivity of olivine aggregates and its implications for the electrical structure of the upper mantle. Earth Planet. Sci. Lett. 288, 291–300.
Yoshino, T., Matsuzaki, T., Yamashita, S., Katsura, T., 2006. Hydrous olivine unable to account for conductivity anomaly at the top of the asthenosphere. Nature 443, 974–976.